\



M1 transition energy and rate in the ground configuration of Ag-like ions with $62 \leq Z \leq 94$

Ju Meng(孟举), Wen-Xian Li(李文显), Ji-Guang Li(李冀光), Ze-Qing Wu(吴泽清), Jun Yan(颜君), Yong Wu(吴勇), and Jian-Guo Wang(王建国)

Citation: Chin. Phys. B, 2022, 31 (**1**): 013101. DOI: 10.1088/1674-1056/ac1333
Journal homepage: http://cpb.iphy.ac.cn; http://iopscience.iop.org/cpb

What follows is a list of articles you may be interested in

Calculations of dynamic multipolar polarizabilities of the Cd clock transition levels

Mi Zhou(周密) and Li-Yan Tang(唐丽艳)
Chin. Phys. B, 2021, 30 (**8**): 083102. DOI: 10.1088/1674-1056/abf0fc

Isotope shift of the 2s $^2S_{1/2}$ $\rightarrow$ 2p $^2P_{1/2,3/2}$ transitions of Li-like Ca ions

Denghong Zhang(张登红), Fangjun Zhang(张芳军), Xiaobin Ding(丁晓彬), and Chenzhong Dong(董晨钟)
Chin. Phys. B, 2021, 30 (**4**): 043102. DOI: 10.1088/1674-1056/abc7a2

Imaging alignment of rotational state-selected CH_3I molecule

Le-Le Song(宋乐乐), Yan-Hui Wang(王艳辉), Xiao-Chun Wang(王晓春), Hong-Tao Sun(孙洪涛), Lan-Hai He(赫兰海), Si-Zuo Luo(罗嗣佐), Wen-Hui Hu(胡文惠), Dong-Xu Li(李东旭), Wen-Hui Zhu(朱文会), Ya-Nan Sun(孙亚楠), Da-Jun Ding(丁大军), Fu-Chun Liu(刘福春)
Chin. Phys. B, 2019, 28 (**2**): 023101. DOI: 10.1088/1674-1056/28/2/023101

Determination of static dipole polarizabilities of Yb atom

Zhi-Ming Tang(唐志明), Yan-Mei Yu(于艳梅), Chen-Zhong Dong(董晨钟)
Chin. Phys. B, 2018, 27 (**6**): 063101. DOI: 10.1088/1674-1056/27/6/063101

Correlation effects on the fine-structure splitting within the $3d^9$ ground configuration in highly-charged Co-like ions

Xue-Ling Guo(郭学玲), Min Huang(黄敏), Jun Yan(颜君), Shuang Li(李双),Kai Wang(王凯), Ran Si(司然), Chong-Yang Chen(陈重阳)
Chin. Phys. B, 2016, 25 (**1**): 013101. DOI: 10.1088/1674-1056/25/1/013101

M1 transition energy and rate in the ground configuration of Ag-like ions with $62 \leq Z \leq 94$

Ju Meng(孟举)[1], Wen-Xian Li(李文显)[2], Ji-Guang Li(李冀光)[1,†], Ze-Qing Wu(吴泽清)[1], Jun Yan(颜君)[1,3], Yong Wu(吴勇)[1,3], and Jian-Guo Wang(王建国)[1]

[1] *National Key Laboratory of Computational Physics, Institute of Applied Physics and Computational Mathematics, Beijing* 100088, *China*
[2] *Key Laboratory of Solar Activity, National Astronomical Observatories, Chinese Academy of Sciences, Beijing* 100012, *China*
[3] *HEDPS, Center for Applied Physics and Technology, and College of Engineering, Peking University, Beijing* 100871, *China*

(Received 11 May 2021; revised manuscript received 3 July 2021; accepted manuscript online 12 July 2021)

Systematic calculations and assessments are performed for the magnetic dipole (M1) transition energies and rates between the $^2F^o_{5/2,7/2}$ levels in the ground configuration $4d^{10}4f$ along the Ag-like isoelectronic sequence with $62 \leq Z \leq 94$ based on the second-order many-body perturbation theory implemented in the Flexible Atomic Code. The electron correlations, Breit interaction and quantum electrodynamics effects are taken into account in the present calculations. The accuracy and reliability of our results are evaluated through comprehensive comparisons with available measurements and other theoretical results. For transition energies, our results are in good agreement with the recent experimental data obtained from the electron beam ion traps within 0.18%. The maximum discrepancy between our results and those obtained with the large-scale multiconfiguration Dirac–Hartee–Fock calculations by Grumer *et al.* [*Phys. Rev. A* **89** 062501 (2014)] is less than 0.13% along the isoelectronic sequence. Furthermore, the corresponding M1 transition rates are also reported. The present results can be used as the benchmark and useful for spectra simulation and diagnostics of astrophysical and fusion plasmas.

Keywords: Ag-like ions, magnetic dipole transition, fine-structure splitting

PACS: 31.15.am, 31.15.ag **DOI:** 10.1088/1674-1056/ac1333

1. Introduction

Tungsten (W) is selected as a plasma-facing material for the International Thermonuclear Experimental Reactor (ITER), a magnetic confinement fusion device, because of its favorable physical, chemical and thermal properties, that is, the high energy threshold of sputtering, low sputtering yield, high re-deposition efficiency, and low tritium retention.[1–4] The W ions including Ag-like W^{27+}, however, cause power loss by radiative emission and then may quench the fusion reactions, if entering into the edge region of plasma.[5] Therefore, the spectroscopic diagnostics of these W ions are critical for the operation of the fusion plasmas. On the other hand, accurate atomic data of these W ions are also essential to acquire the state of the fusion plasma such as electron densities and temperatures. Moreover, Ag-like ions, e.g., Nd^{13+} and Sm^{15+}, have been proposed as candidates for the development of the next generation atomic clocks due to their long-lived metastable states, transition wavelengths in optical range, and sensitivity to variation of the fine-structure constant.[6–8] In addition, theoretical investigation on the simple ground states of Ag-like ions can also be useful to test the quantum electrodynamics (QED) effects.

Measurements and theoretical calculations have been performed on the magnetic dipole (M1) transition energies and rates in the ground configuration $4d^{10}4f$ of Ag-like ions. Sugar and Kaufman[9] obtained the excitation energies of Ag-like ions ($Z = 58$–67, 74) with a high-voltage-triggered spark and photographed on the NBS 10.7 m grazing incidence spectrograph in the early 1980s. Over the past decades, most of the experiments were carried out by using the electron beam ion traps (EBITs), through which one could directly measure the fine-structure splittings in the ground configuration. For instance, Fei *et al.*[10] observed the M1 transition of Ag-like W ($Z = 74$) using the Shanghai permanent magnet electron beam ion trap (SH-PermEBIT). Subsequently, Zhao *et al.*[11] reported the wavelength for the M1 transition of Ag-like Yb ($Z = 70$) with the same experimental facility. Murata *et al.*[12] identified the M1 lines of Ag-like Ho ($Z = 67$), Er ($Z = 68$) and Tm ($Z = 69$) ions by employing the compact electron beam ion trap (CoBIT) in Tokyo-EBIT laboratory.[13] In theory, Safronova *et al.*[14] calculated the fine-structure splitting of the $4f\ ^2F^o$ term for certain Ag-like ions at the neutral end using the relativistic many-body perturbation theory (RMBPT). Ivanova[15,16] reported the energy separations in Ag-like ions with $50 \leq Z \leq 86$ based on the relativistic perturbation theory with a model potential (RPTMP). In the framework of the multi-configuration Dirac–Hartree–Fock (MCDHF) method, Ding *et al.*[17] gave the M1 transition energies along the Ag-like isoelectronic sequence, in which only the core-valence (CV) correlation related to electrons in the 4d core subshell was included. Subsequently, Grumer *et al.*[18] reevaluated the

†Corresponding author. E-mail: li_jiguang@iapcm.ac.cn
© 2022 Chinese Physical Society and IOP Publishing Ltd

wavelengths and calculated the corresponding transition rates in Ag-like ions with $50 \leq Z \leq 94$ based on the large-scale multiconfiguration Dirac–Hartee–Fock (MCDHF) calculations. In particular, they considered the effect of the CV correlation with $n = 4$ and $n = 3$ shells and pointed out the importance of these deep-core-valence correlations. Besides the systematic calculations for Ag-like ions along the isoelectronic sequence, there are also some investigations for a few individual ions.[6–8,19,20] Dzuba *et al.*[8] and Safronova *et al.*[6,7] used the correlation potential method and the relativistic linearized coupled-cluster method with inclusion of all single, double, and partial triple excitations (SDpT), respectively, to obtain the transition energies for Ag-like Nd^{13+} and Sm^{15+}. Safronova *et al.*[19,20] also made a detailed study on the atomic parameters of Ag-like W ($Z = 74$) ion employing the RMBPT method.

As mentioned above, the calculated M1 transition energies in the ground configuration of Ag-like ions are mainly obtained with the MCDHF and RMBPT methods. These two methods are based on different theoretical approximations, that is, the variational principle and perturbation theory, respectively. Comparison of these two results can provide a reliable evaluation of accuracy for the atomic data of Ag-like ions. However, the difference in the fine-structure splittings is obvious for the low-Z ions between the MCDHF[18] and the RMBPT[14] calculations, although the agreement becomes better at the high-Z end of the sequence. Therefore, it is necessary to carry out a new calculation, especially for the low-Z ions in the Ag-like isoelectronic sequence, to provide more reliable and accurate atomic data.

In the present work, we have performed systematic calculations on the M1 transition energies and rates in the ground configuration $4d^{10}4f$ of Ag-like ions between $Z = 62$ and 94 using the second-order RMBPT implemented in the Flexible Atomic Code (FAC).[21] In order to evaluate the reliability of the present RMBPT results, extensive comparisons have been made with the available experimental data, as well as with the previous theoretical results. The data in the present work is useful for the spectral simulation and plasma diagnostics.

2. Theoretical method

In the present work, the second-order RMBPT is adopted to perform the calculations. This method was implemented within the FAC package by Gu[22–25] and has been widely used in atomic structure calculations. The details of the RMBPT method can be found elsewhere.[26–30] Here, we only give a brief description.

The Hamiltonian of a many-electron atomic system with N electrons is written in the Dirac–Coulomb–Breit (DCB) approximation[31] as

$$H_{\rm DCB} = \sum_{i}^{N} h_{\rm d}(i) + \sum_{i<j}^{N} \left(\frac{1}{r_{ij}} + B_{ij} \right), \tag{1}$$

where $h_{\rm d}(i)$ is the one-electron Dirac Hamiltonian in which the electron kinetic energy, the resting energy, and the coulomb interaction between electrons and the nuclei are included, B_{ij} is the frequency-independent Breit interaction,

$$B_{ij} = -\frac{1}{2r_{ij}} \left[\boldsymbol{\alpha}_i \cdot \boldsymbol{\alpha}_j + \frac{(\boldsymbol{\alpha}_i \cdot \boldsymbol{r}_{ij}) \cdot (\boldsymbol{\alpha}_j \cdot \boldsymbol{r}_{ij})}{\boldsymbol{r}_{ij}^2} \right], \tag{2}$$

where $\boldsymbol{\alpha}_i$ is the Dirac matrices. Starting with the central-field approximation, the electron correlation is treated as perturbation, i.e.,

$$V = \frac{1}{2} \sum_{i \neq j}^{N} \frac{1}{r_{ij}} - \sum_{i=1}^{N} U(r_i). \tag{3}$$

Here, $U(r)$ is the Hartree–Fock potential.

As described in Ref. [32], the complete eigenfunction space of the full Hamiltonian is partitioned into two subspaces labeled M and N. The wave operator Ω is defined to transform the model functions in M space to the eigenfunctions of full Hamiltonian of the system,

$$\Psi_k = \Omega \Psi_k^0. \tag{4}$$

With the projection operator

$$P = \sum_{k \in M} |\Phi_k\rangle \langle \Phi_k|, \tag{5}$$

and the wave operator, the Schrödinger equation of the system can be written as

$$H_{\rm eff} \Psi_k^0 = E_k \Psi_k^0, \tag{6}$$

where $H_{\rm eff}$ is the effective Hamiltonian in the model space

$$H_{\rm eff} = P H_0 P + PV\Omega. \tag{7}$$

From Eq. (6), we know that the eigenvalues and eigenfunctions of $H_{\rm eff}$ are the exact energies and the model functions, respectively. This means that the true energies of the system can be obtained by solving the eigenvalue problem of an effective Hamiltonian $H_{\rm eff}$ in the model space M. The wave operator Ω satisfies the operator relation

$$[\Omega, H_0] = V\Omega - \Omega V \Omega, \tag{8}$$

from which we can obtain each order expansion of Ω through a perturbation approach. Then, the expansion of $PV\Omega$ and $H_{\rm eff}$ are determined.

In the present calculation, the expansion of Ω is retained to the first order. Then the effective Hamiltonian is given by

$$\langle \Phi_i | H_{\rm eff} | \Phi_j \rangle = \langle \Phi_i | H_{\rm DCB} | \Phi_j \rangle + \sum_{r \in N} \frac{\langle \Phi_i | V | \Phi_r \rangle \langle \Phi_r | V | \Phi_j \rangle}{E_j^0 - E_r^0} \tag{9}$$

in terms of matrix elements in the model space M.

By solving Eq. (6), we can obtain the total energy of the system as follows:

$$E_k = E_k^{\rm CI} + E_k^{(2)}, \tag{10}$$

where $E_k^{\rm CI}$ is the eigenvalues of $PH_{\rm DCB}P$ in the model space with the corresponding eigenvectors b_{ki}^0, and $E_k^{(2)}$ is the second-order energy correction from the correlations of N space,

$$E_k^{(2)} = \sum_{r\in N}\sum_{i,j\in M} b_{ki}^0 b_{kj}^0 \frac{\langle \Phi_i|V|\Phi_r\rangle \langle \Phi_r|V|\Phi_j\rangle}{E_j^0 - E_r^0}. \tag{11}$$

The Dirac–Fock–Slater approximation is employed to produce the function basis $\{\Phi_r\}$. This means that the central potential $U(r)$ in Eq. (3) is a modified Dirac–Fock–Slater potential including the spherically averaged potential due to bound electrons, and the local approximations to the exchange interactions excluding the self-interaction term. Furthermore, one-electron radial orbitals can be obtained by the self-consistent field procedures.

In the present work, the M space includes the states belonging to $4d^{10}4f$, while the N space consists of all possible configurations generated by single and double excitation from each occupied orbital of the configurations in the M space. For one-electron excitation, the maximum principal quantum number n values is set to 170, and for double excitation, the maximum n values to 65. In addition, the maximum orbital angular quantum number is set to $l = 30$. The extrapolation beyond the maximum n values is carried out for building the effective Hamiltonian. In addition, several small higher order QED effects are also taken into account in the present calculations, including the vacuum polarization and self-energy. In order to evaluate the accuracy of our calculations, we also investigated the convergence of atomic parameters concerned by increasing the N space as discussed in Ref. [30]. For example, we performed an additional calculation for Ag-like Sm ($Z = 62$) and Ag-like Eu ($Z = 63$), in which we set the maximal n values for single and double excitations up to be 225 and 80, respectively. We found a good agreement between these two calculations and the difference is less than 0.01%.

3. Result and discussion

3.1. Fine-structure energy levels

The resulting M1 transition energies from the present RMBPT calculations for ions in Ag-like isoelectronic sequence with $62 \le Z \le 94$ are shown in Fig. 1. It is clear that the fine-structure energy separations increase rapidly and smoothly along the isoelectronic sequence. This confirms the argument by Grumer *et al.* in Ref. [18].

In Table 1, we present our RMBPT results of the fine-structure energy separations for the isoelectronic sequence as well as other available theoretical and experimental data. The $\text{Expt}_{\rm DIR}$ represents energy separations measured directly by the observation of the 4f $^2F^{\rm o}_{7/2} \rightarrow {}^2F^{\rm o}_{5/2}$ M1 transition lines.[10–12] These experiments were performed by using the EBIT facilities, including the CoBIT[13] in Tokyo-EBIT laboratory and SH-Perm EBIT[33] at the Shanghai EBIT laboratory. The $\text{Expt}_{\rm IND}$ stands for the indirect measurements, that is, the transition energies are deduced from the other transitions involving the higher excited levels.[9] The values in the brackets are based on the interpolated values of 4f $^2F^{\rm o}_{7/2}$.[9] The available theoretical works for Ag-like ions, that is, the MCDHF calculations (hereafter referred to as MCDHF1) by Grumer *at al.*,[18] the RMBPT calculations (RMBPT2) by Safronova *et al.*,[14] the MCDHF calculations (MCDHF2) by Ding *et al.*,[17] and Ivanova's results based on RPTMP,[15,16] are also displayed for comparison. In Fig. 2, we illustratively show the differences of the fine-structure separation obtained by the present RMBPT calculations from other theoretical and experimental data. It is clear that our results are in excellent agreement with the direct measurements; the relative deviations between our results and the direct experiments are -0.16%, -0.13%, -0.11%, -0.06% and -0.03%, respectively, for the ions with $Z = 67$, 68, 69, 70, and 74. The deviations decrease with increase of Z along the isoelectronic sequence. It should be stressed that these direct measurements were performed only for the Ag-like ions with high Z. As point out in Ref. [11], for the ions with lower Z, the M1 transition lines lie in the infrared range and the corresponding transition probabilities are very small, which may make the direct measurement of the M1 transitions more difficult. Compared with the indirect measurements[9] for the lower-Z Ag-like ions, the deviations between our results and indirect experimental values become larger than those in high-Z ions from the direct experiments. Moreover, we find that these indirect experimental data show an irregular trend along with the isoelectronic sequence. Therefore, we argue that the larger deviations may arise from the experimental errors, but it requires further measurements with higher precision.

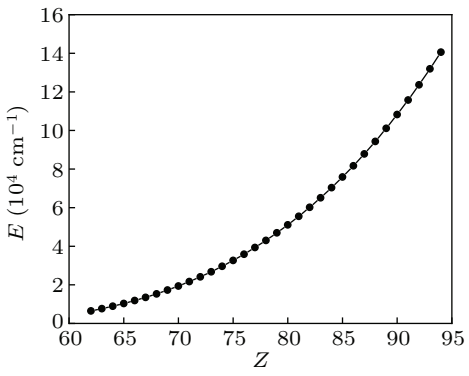


Fig. 1. Energies of the $4d^{10}4f\ {}^2F^{\rm o}$ fine-structure separation along the Ag-like isoelectronic sequence as a function of nuclear charge Z.

Table 1. Comparisons of the present 4f $^2F^o_{5/2,7/2}$ fine-structure splitting with the experimental data and previous theoretical data from different methods MCDHF1,[18] RMBPT2,[14] MCDHF2,[17] RPTMP.[15,16] The Expt_{DIR} and Expt_{IND} are directly and indirectly measured fine-structure energies, respectively. In the column of Expt_{IND}, the values in the brackets are based on the interpolated values of 4f $^2F^o_{7/2}$. All energies are given in cm^{-1}.

Z	Ions	Present	MCDHF1[a]	RMBPT2[b]	MCDHF2[c]	RPTMP[d]	Expt_{IND}	Expt_{DIR}
62	Sm^{15+}	6472	6463	6533	6301	6353	6555[e]	
63	Eu^{16+}	7635	7628	7697	7444	7504	7521[e]	
64	Gd^{17+}	8913	8909	8977	8685	8800	[8900[e]]	
65	Tb^{18+}	10314	10311	10378	10033	10225	10280[e]	
66	Dy^{19+}	11843	11842	11908	11512	11870	11770[e]	
67	Ho^{20+}	13508	13509	13573	13140	13486	[13500[e]]	13487 ± 2[f]
68	Er^{21+}	15317	15320	15383	14926	15371		15297 ± 2[f]
69	Tm^{22+}	17277	17280	17341	16871	17695		17258 ± 2[f]
70	Yb^{23+}	19395	19399	19459	18979	19848		19383 ± 4[g]
71	Lu^{24+}	21679	21685	21741	21254	22465		
72	Hf^{25+}	24138	24145	24198	23702	25285		
73	Ta^{26+}	26778	26786	26838	26331	28350		
74	W^{27+}	29609	29619	29668	29151	31769		29600 ± 2[h]
75	Re^{28+}	32638	32651	32696	32167	35494		
76	Os^{29+}	35877	35890	35932	35390	39491		
77	Ir^{30+}	39331	39346	39385	38828	43765		
78	Pt^{31+}	43011	43028	43063	42491	48320		
79	Au^{32+}	46927	46945	46976	46387	53411		
80	Hg^{33+}	51086	51106	51133	50527	58754		
81	Tl^{34+}	55498	55521	55542	54918	64649		
82	Pb^{35+}	60174	60199	60216	59573	70791		
83	Bi^{36+}	65122	65151	65162	64499	77338		
84	Po^{37+}	70356	70385	70391	69708	84066		
85	At^{38+}	75866	75914	75914	75209	91483		
86	Rn^{39+}	81696	81747	81741	81012	99145		
87	Fr^{40+}	87840	87894		87129			
88	Ra^{41+}	94310	94366		93571			
89	Ac^{42+}	101115	101175		100347			
90	Th^{43+}	108268	108331		107469			
91	Pa^{44+}	115778	115845		114944			
92	U^{45+}	123658	123729		122792			
93	Np^{46+}	131919	131995					
94	Pu^{47+}	140573	140654					

[a]From Table 1 in Ref. [18], [b]deduced from Table 11 in Ref. [15], [c]from Table 2 in Ref. [17], [d]deduced from Table 3 in Ref. [15], [e]from Table 3 in Ref. [9], [f]from Table 3 in Ref. [12], [g]deduced from Table 3 in Ref. [11], [h]from Table 3 in Ref. [10].

On the theoretical side, we compare our RMBPT calculations with the two existing MCDHF results[17,18] and the previous RMBPT2 calculations.[14] As shown in Fig. 2, our RMBPT calculations are in excellent agreement with MCDHF1 and RMBPT2 calculations for heavy Ag-like ions. For ions with $Z \geq 78$, the relative deviations between these three results are less than 0.1%. As the nuclear charge Z decreases, our RMBPT results and the MCDHF1 calculation still agree very well, and the largest difference is about 0.13% for Ag-like Sm ($Z = 62$). However, the RMBPT2 results deviate from those by MCDHF1 and the present RMBPT results with decreasing Z along the isoelectronic sequence. Recently, Safronova *et al.*[6,7] performed a new calculation for Ag-like Sm^{15+} by employing the relativistic linearized coupled-cluster (CC) method and including all single, double, and partial triple excitations (SDpT). The relative difference between the present RMBPT calculations and their SDpT CC calculations for Ag-like Sm^{15+} reduces to 0.43%, which is much smaller than that of the RMBPT2 results. From Fig. 2 we also observe that the discrepancies between the present and the MCDHF2 results are much larger than that from the MCDHF1 results and the latter has an irregular isoelectronic behavior. This may be due to the fact that only the CV correlation with 4*d* subshell is included in the MCDHF2 calculations while the MCDHF1 and the present calculations consider the CV correlation with $n = 3$, 4 shells. On the other hand, the deep-core-valence correlation contributes greatly to the final energy separations.[18] As discussed above, we believe that our RMBPT values and MCDHF1 values are more accurate compared with the MCDHF2 and RMBPT2 results, especially for the lower-Z Ag-like ions. Finally, we compare our RMBPT calculations with the ones obtained with the RPTMP method.[15,16]

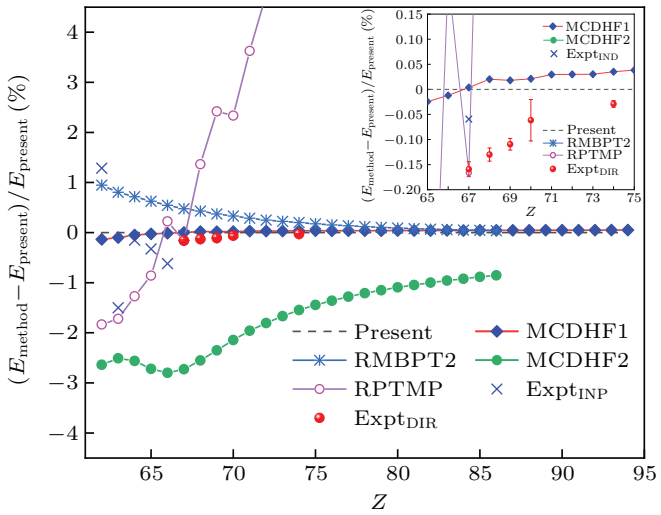


Fig. 2. Percentage differences between the present and other theoretical and experimental fine-structure splittings of the Ag-like isoelectronic sequence as a function of atomic number Z. The Expt$_{\rm DIR}$ and Expt$_{\rm IND}$ represent directly and indirectly measured energy separations, respectively. Error bars of the direct experimental data points are available and included in the plot. The MCDHF1,[18] RMBPT2,[14] MCDHF2[17] and RPTMP[15,16] are earlier calculations.

As shown in Fig. 2, the isoelectronic trend of RPTMP results[15,16] exhibits a significant deviation from our RMBPT calculations and other theoretical values. The inexplicable disagreement may arise from the inappropriate choice of the experimental reference values for the empirical model potentials used in the RPTMP calculations. Based on the above discussions, we suggest that the transition energies from the present calculations and MCDHF1 should be used as a reference.

3.2. Wavelengths and transition probabilities

In Table 2, we present the calculated (vacuum) wavelengths, transition rates and weighted oscillator strengths for M1 transitions between fine-structure energy levels in the $4d^{10}4f$ ground configurations of Ag-like ions along the isoelectronic sequence. The MCDHF1 calculations[18] are also given for comparation. In Fig. 3, we compared the A values of the M1 transition obtained from the present RMBPT and those from the MCDHF1 method along the isoelectronic sequence. The differences of these two calculations decrease smoothly along the sequence, from 12.4% for $Z=62$ to 5.4% for $Z=94$. As shown in Table 2, the M1 transition rates are rather small, especially for the low-Z ions. For such weak transitions, the agreement between the two independent calculations is satisfactory.

Table 2. Wavelength λ (Å), transition rates A (s^{-1}) and oscillator strength gf of the M1 transition between $4f\ ^2F^{\rm o}_{5/2}$ and $^2F^{\rm o}_{7/2}$ in Ag-like ions with $62 \le Z \le 94$, the MCDHF1 results[18] are also listed for comparison.

		RMBPT			MCDHF1[a]		
Z	Ions	λ	A	gf	λ	A	gf
62	Sm^{15+}	1.545×10^{4}	2.730×10^{0}	7.817×10^{-7}	1.547×10^{4}	3.117×10^{0}	8.949×10^{-7}
63	Eu^{16+}	1.310×10^{4}	4.513×10^{0}	9.283×10^{-7}	1.311×10^{4}	5.124×10^{0}	1.056×10^{-6}
64	Gd^{17+}	1.122×10^{4}	7.220×10^{0}	1.090×10^{-6}	1.123×10^{4}	8.161×10^{0}	1.233×10^{-6}
65	Tb^{18+}	9.696×10^{3}	1.124×10^{1}	1.268×10^{-6}	9.698×10^{3}	1.265×10^{1}	1.427×10^{-6}
66	Dy^{19+}	8.443×10^{3}	1.711×10^{1}	1.463×10^{-6}	8.444×10^{3}	1.916×10^{1}	1.639×10^{-6}
67	Ho^{20+}	7.403×10^{3}	2.550×10^{1}	1.676×10^{-6}	7.402×10^{3}	2.845×10^{1}	1.869×10^{-6}
68	Er^{21+}	6.529×10^{3}	3.731×10^{1}	1.907×10^{-6}	6.528×10^{3}	4.148×10^{1}	2.120×10^{-6}
69	Tm^{22+}	5.788×10^{3}	5.375×10^{1}	2.160×10^{-6}	5.787×10^{3}	5.952×10^{1}	2.391×10^{-6}
70	Yb^{23+}	5.156×10^{3}	7.629×10^{1}	2.432×10^{-6}	5.155×10^{3}	8.420×10^{1}	2.683×10^{-6}
71	Lu^{24+}	4.613×10^{3}	1.069×10^{2}	2.727×10^{-6}	4.612×10^{3}	1.176×10^{2}	2.999×10^{-6}
72	Hf^{25+}	4.143×10^{3}	1.479×10^{2}	3.045×10^{-6}	4.142×10^{3}	1.623×10^{2}	3.339×10^{-6}
73	Ta^{26+}	3.734×10^{3}	2.025×10^{2}	3.388×10^{-6}	3.733×10^{3}	2.216×10^{2}	3.703×10^{-6}
74	W^{27+}	3.377×10^{3}	2.745×10^{2}	3.755×10^{-6}	3.376×10^{3}	2.995×10^{2}	4.094×10^{-6}
75	Re^{28+}	3.064×10^{3}	3.685×10^{2}	4.149×10^{-6}	3.063×10^{3}	4.011×10^{2}	4.513×10^{-6}
76	Os^{29+}	2.787×10^{3}	4.906×10^{2}	4.571×10^{-6}	2.786×10^{3}	5.326×10^{2}	4.960×10^{-6}
77	Ir^{30+}	2.542×10^{3}	6.477×10^{2}	5.021×10^{-6}	2.542×10^{3}	7.017×10^{2}	5.436×10^{-6}
78	Pt^{31+}	2.325×10^{3}	8.487×10^{2}	5.502×10^{-6}	2.324×10^{3}	9.175×10^{2}	5.944×10^{-6}
79	Au^{32+}	2.131×10^{3}	1.104×10^{3}	6.014×10^{-6}	2.130×10^{3}	1.191×10^{3}	6.484×10^{-6}
80	Hg^{33+}	1.957×10^{3}	1.427×10^{3}	6.558×10^{-6}	1.957×10^{3}	1.537×10^{3}	7.057×10^{-6}
81	Tl^{34+}	1.802×10^{3}	1.833×10^{3}	7.136×10^{-6}	1.801×10^{3}	1.970×10^{3}	7.666×10^{-6}
82	Pb^{35+}	1.662×10^{3}	2.340×10^{3}	7.750×10^{-6}	1.661×10^{3}	2.511×10^{3}	8.310×10^{-6}
83	Bi^{36+}	1.536×10^{3}	2.970×10^{3}	8.399×10^{-6}	1.535×10^{3}	3.182×10^{3}	8.992×10^{-6}
84	Po^{37+}	1.421×10^{3}	3.750×10^{3}	9.087×10^{-6}	1.421×10^{3}	4.012×10^{3}	9.712×10^{-6}
85	At^{38+}	1.318×10^{3}	4.709×10^{3}	9.811×10^{-6}	1.317×10^{3}	5.032×10^{3}	1.047×10^{-5}
86	Rn^{39+}	1.224×10^{3}	5.887×10^{3}	1.058×10^{-5}	1.223×10^{3}	6.283×10^{3}	1.128×10^{-5}
87	Fr^{40+}	1.138×10^{3}	7.326×10^{3}	1.139×10^{-5}	1.138×10^{3}	7.807×10^{3}	1.212×10^{-5}
88	Ra^{41+}	1.060×10^{3}	9.078×10^{3}	1.224×10^{-5}	1.060×10^{3}	9.660×10^{3}	1.301×10^{-5}
89	Ac^{42+}	9.890×10^{2}	1.120×10^{4}	1.314×10^{-5}	9.884×10^{2}	1.190×10^{4}	1.395×10^{-5}
90	Th^{43+}	9.236×10^{2}	1.376×10^{4}	1.408×10^{-5}	9.231×10^{2}	1.461×10^{4}	1.493×10^{-5}
91	Pa^{44+}	8.637×10^{2}	1.685×10^{4}	1.507×10^{-5}	8.632×10^{2}	1.786×10^{4}	1.596×10^{-5}
92	U^{45+}	8.087×10^{2}	2.055×10^{4}	1.611×10^{-5}	8.082×10^{2}	2.176×10^{4}	1.705×10^{-5}
93	Np^{46+}	7.580×10^{2}	2.497×10^{4}	1.721×10^{-5}	7.576×10^{2}	2.641×10^{4}	1.818×10^{-5}
94	Pu^{47+}	7.114×10^{2}	3.024×10^{4}	1.835×10^{-5}	7.110×10^{2}	3.195×10^{4}	1.937×10^{-5}

[a]From Table 3 in Ref. [18].

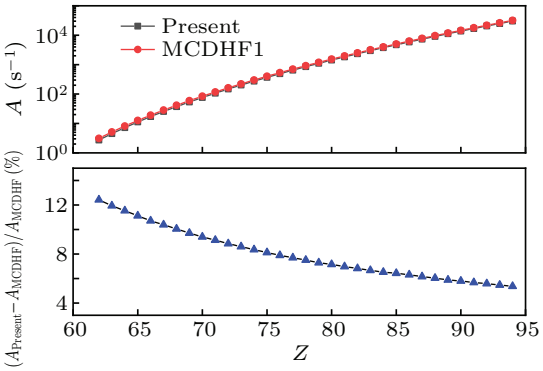


Fig. 3. Comparisons of the present calculated rates with those of the MCDHF1 calculations for the M1 4f $^2F^{\rm o}_{5/2}$–$^2F^{\rm o}_{7/2}$ transition along the Ag-like isoelectronic sequence. The top panel shows the present A-values and those from MCDHF1 and the bottom one is the differences between these two calculations.

4. Conclusions

In summary, we have calculated the M1 transition energies and rates in the ground configuration $4d^{10}4f$ of Ag-like ions between $Z = 62$ and $Z = 94$ using the second-order RMBPT approach implemented in the FAC code. The present RMBPT energy separations show a smooth Z-dependence, and agree very well with the direct experimental data obtained from EBIT devices. The relative differences are less than 0.08% for Ag-like Yb^{23+} and W^{27+}, within 0.17% for Ag-like Ho^{20+}, Er^{21+} and Tm^{22+}. Extensive comparisons of our wavelengths and rates for the M1 transition with the most recent large-scale MCDHF1 results[18] show that these two results are in good agreement with each other. For the fine-structure splittings, the maximum deviation between our RMBPT and the MCDHF1 results is less than 0.13%. For the transition rates, the relative discrepancies are less than $\sim$ 13% for all Ag-like ions concerned. We also demonstrate that for the ions at the beginning of the Ag-like isoelectronic sequence, our RMBPT and MCDHF1 results are more accurate than other theoretical values. Therefore, we believe that these two independent theoretical calculations can be used as the benchmark for the atomic data of Ag-like ions and will be useful for the line identifications of experimental spectra, as well as for the plasma spectra modeling and diagnostics in the fusion-plasma community.

Acknowledgements

This work is supported by the National Natural Science Foundation of China (Grant Nos. 11874090, 11934004, 11404180, 11604052, and 11774037), and the National Key Research and Development Program of China (Grant No. 2017YFA0402300).

References

[1] Skinner C H 2008 *Can. J. Phys.* **86** 285
[2] Neu R, Dux R, Kallenbach A, Putterich T, Balden M, Fuchs J C, Herrmann A, Maggi C F, O'Mullane M, Pugno R, Radivojevic I, Rohde V, Sips A C C, Suttrop W, Whiteford A and team A U 2005 *Nucl. Fusion* **45** 209
[3] Matthews G F, Coad P, Greuner H, Hill M, Hirai T, Likonen J, Maier H, Mayer M, Neu R, Philipps V, Pitts R, Riccardo V and Contributors J E 2009 *J. Nucl. Mater.* **390–391** 934
[4] Qiu M L, Li W X, Zhao Z Z, Yang Y, Xiao J, Brage T, Hutton R and Zou Y 2015 *J. Phys. B: At. Mol. Opt. Phys.* **48** 144029
[5] Biedermann C, Radtke R, Seidel R and Putterich T 2009 *Phys. Scr.* **2009** 014026
[6] Safronova M S, Dzuba V A, Flambaum V V, Safronova U I, Porsev S G and Kozlov M G 2014 *Phys. Rev. A* **90** 042513
[7] Safronova M S, Dzuba V A, Flambaum V V, Safronova U I, Porsev S G and Kozlov M G 2014 *Phys. Rev. Lett.* **113** 030801
[8] Dzuba V A, Derevianko A and Flambaum V V 2012 *Phys. Rev. A* **86** 054502
[9] Sugar J and Kaufman V 1981 *Phys. Scr.* **24** 742
[10] Fei Z, Zhao R, Shi Z, Xiao J, Qiu M, Grumer J, Andersson M, Brage T, Hutton R and Zou Y 2012 *Phys. Rev. A* **86** 062501
[11] Zhao R, Grumer J, Li W, Xiao J, Brage T, Huldt S, Hutton R and Zou Y 2014 *J. Phys. B: At. Mol. Opt. Phys.* **47** 185004
[12] Murata S, Nakajima T, Safronova M S, Safronova U I and Nakamura N 2017 *Phys. Rev. A* **96** 062506
[13] Nakamura N, Kikuchi H, Sakaue H A and Watanabe T 2008 *Rev. Sci. Instrum.* **79** 063104
[14] Safronova U I, Savukov I M, Safronova M S and Johnson W R 2003 *Phys. Rev. A* **68** 062505
[15] Ivanova E P 2011 *At. Data Nucl. Data Tables* **97** 1
[16] Ivanova E P 2009 *At. Data Nucl. Data Tables* **95** 786
[17] Ding X B, Koike F, Murakami I, Kato D, Sakaue H A, Dong C Z and Nakamura N 2012 *J. Phys. B: At. Mol. Opt. Phys.* **45** 035003
[18] Grumer J, Zhao R F, Brage T, Li W X, Huldt S, Hutton R and Zou Y M 2014 *Phys. Rev. A* **89** 062511
[19] Safronova U I, Safronova A S, Beiersdorfer P and Johnson W R 2011 *J. Phys. B: At. Mol. Opt. Phys.* **44** 035005
[20] Safronova U I and Safronova A S 2010 *J. Phys. B: At. Mol. Opt. Phys.* **43** 074026
[21] Gu M F 2008 *Can. J. Phys.* **86** 675
[22] Gu M F 2007 *Astrophys. J. Suppl. Ser.* **169** 154
[23] Gu M F, Holczer T, Behar E and Kahn S M 2006 *Astrophys. J.* **641** 1227
[24] Gu M F 2005 *At. Data Nucl. Data Tables* **89** 267
[25] Gu M F 2005 *Astrophys. J. Suppl. Ser.* **156** 105
[26] Li W, Xiao J, Shi Z, Fei Z, Zhao R, Brage T, Huldt S, Hutton R and Zou Y 2016 *J. Phys. B: At. Mol. Opt. Phys.* **49** 105002
[27] Wang K, Guo X L, Liu H T, Li D F, Long F Y, Han X Y, Duan B, Li J G, Huang M, Wang Y S, Hutton R, Zou Y M, Zeng J L, Chen C Y and Yan J 2015 *Astrophys. J. Suppl. Ser.* **218** 16
[28] Guo X L, Huang M, Yan J, Li S, Si R, Li C Y, Chen C Y, Wang Y S and Zou Y M 2015 *J. Phys. B: At. Mol. Opt. Phys.* **48** 144020
[29] Wang K, Li D F, Liu H T, Han X Y, Duan B, Li C Y, Li J G, Guo X L, Chen C Y and Yan J 2014 *Astrophys. J. Suppl. Ser.* **215** 26
[30] Fei Z, Li W, Grumer J, Shi Z, Zhao R, Brage T, Huldt S, Yao K, Hutton R and Zou Y 2014 *Phys. Rev. A* **90** 052517
[31] Sucher J 1980 *Phys. Rev. A* **22** 348
[32] Lindgren I 1974 *J. Phys. B: At. Mol. Opt. Phys.* **7** 2441
[33] Shi Z, Zhao R F, Li W X, Tu B S, Yang Y, Xiao J, Huldt S, Hutton R and Zou Y M 2014 *Rev. Sci. Instrum.* **85** 063110